Available online at www.sciencedirect.com

ScienceDirect

Procedia Computer Science 138 (2018) 388–392

Procedia Computer Science

www.elsevier.com/locate/procedia

CENTERIS - International Conference on ENTERprise Information Systems / ProjMAN - International Conference on Project MANagement / HCist - International Conference on Health and Social Care Information Systems and Technologies, CENTERIS/ProjMAN/HCist 2018

Sentinel-1A/B imagery for terrain deformation monitoring: a strategy for Atmospheric Phase Screening (APS) estimation

M. Cuevas-González[a,*], M. Crosetto[a], O. Monserrat[a], B. Crippa[b]

[a]*Centre Tecnològic de Telecomunicacions de Catalunya (CTTC/CERCA), Division of Geomatics, Av. Gauss 7, E-08860, Castelldefels (Barcelona), Spain*

[b]*Department of Geophysics, University of Milan, Via Cicognara 7, I-20129, Milan, Italy*

Abstract

This work focus on terrain deformation monitoring by means of C-band Synthetic Aperture Radar (SAR) Sentinel-1A/B imagery exploiting the Persistent Scatterer Interferometry (PSI) technique. The deformation monitoring strategy described in this article is related to a specific monitoring scenario where a relatively small urban area is potentially affected by deformation and its surroundings are stable. In the case study considered in this work, the scenario corresponds to an area of potential subsidence induced by underground water pumping covering an area of interest with a radius of approximately 1 km. The proposed monitoring strategy takes advantage of the specific scenario at hand and, in particular, of the availability of stable areas in the vicinity of the area potentially affected by ground deformation, to estimate the Atmospheric Phase Screen (APS), i.e. signal propagation delay caused by the Earth's atmosphere, in an attempt to minimize the underestimation of the deformation rate.

Selection and peer-review under responsibility of the scientific committee of the CENTERIS - International Conference on ENTERprise Information Systems / ProjMAN - International Conference on Project MANagement / HCist - International Conference on Health and Social Care Information Systems and Technologies.

Keywords: PSI; APS; Ground deformation; Urban area

* Corresponding author. Tel.: +34-93-645-29-00 ; fax: +34-93-645-29-01.
E-mail address: maria.cuevas@cttc.es

Selection and peer-review under responsibility of the scientific committee of the CENTERIS - International Conference on ENTERprise Information Systems / ProjMAN - International Conference on Project MANagement / HCist - International Conference on Health and Social Care Information Systems and Technologies.
10.1016/j.procs.2018.10.055

1. Introduction

The Persistent Scatterer Interferometry (PSI) technique represents an advanced category of the differential interferometric Synthetic Aperture Radar (DInSAR) techniques. PSI exploits a set of multiple SAR images acquired over the same geographical area to, by means of appropriate processing tools, isolate the deformation signal of interest from the other components contained within the PSI observations, such as the Residual Topographic Error (RTE) component, the Atmospheric Phase Screening (APS) component and the phase noise. See Crosetto et al. (2016) for a comprehensive review of the PSI technique.

PSI techniques have experienced major developments since they were first proposed almost two decades ago (Ferretti et al., 2001), when they were mainly related to C-band imagery such as ERS-1/2, Envisat and Radarsat sensors. The advent of very high resolution X-band data (TerraSAR-X and CosmoSkyMed) in 2007 enabled a major step forward for this kind of techniques and innovative approaches were proposed (Strozzi et al., 2009; Crosetto et al., 2010; Gernhardt and Bamler, 2012; Lan et al., 2012).

The new generation of C-band data acquired by the sensors on board the Sentinel-1A and 1B satellites represents a new wave of further developments, whose potential is already being analysed and some case studies are available in the literature. For example, Sentinel-1 based PSI has been exploited for several applications such as landslide detection and mapping (Barra et al., 2016 and 2017), monitoring of a mega-landslide (Dai et al., 2016), volcano monitoring (González et al., 2015; De Luca et al., 2016), terrain subsidence monitoring (Crosetto et al., 2015; Shirzaei et al., 2017) or infrastructure monitoring (Huang et al., 2017).

The focus of this work is terrain deformation monitoring by means of the PSI technique and C-band Sentinel-1A/B imagery. In particular, an urban area located in Barcelona, Spain (Fig. 1) was analysed and a specific monitoring scenario is considered by assuming that the area to be monitored, potentially affected by subsidence induced by underground water pumping, is surrounded by a stable area. A strategy to estimate the APS component using an external area while minimizing the impact on the terrain deformation estimates is described. This approach was successfully used by Crosetto et al. (2014) using ground-based SAR observations and was first described in Crosetto et al (2002) using DInSAR observations. The main advantage of the approach is to avoid filtering the APS based on a set of spatial and temporal filters.

2. Methodology

The input data used in this work include a stack of 43 co-registered SAR Sentinel-1 images (Table 1), the amplitude dispersion (DA) and a redundant network of 487 wrapped interferograms, generated using most of the 43 Sentinel-1 images as master images (not only single master or consecutive). The main processing stages of the PSI chain proposed in this work are briefly described in this section:

1. 2+1D phase unwrapping of the redundant interferograms (Devanthéry et al., 2014). A spatial 2D phase unwrapping is performed over the redundant set of interferograms followed by a pixel wise 1D phase unwrapping, which uses a robust iterative least squares procedure. This procedure works on the so-called residuals of the interferometric observation equations (with one residual per each of the M interferograms), and fully exploits the integer nature of the unwrapping errors. This stage generates a set of N unwrapped phase images, which are temporally ordered in correspondence with the dates of the SAR images processed.
2. Identification of a stable area in the surroundings of the area of interest.
3. APS component estimation using the stable area. The APS component of the image phases is modelled using a linear model and masking the deformation area.
4. Removal of the estimated APS component from the original single-look interferograms.
5. Estimation of linear deformation velocity and RTE using the periodogram (Biescas et al., 2007).
6. Removal of the residual topographic error from the original single-look interferograms.
7. 2+1D phase unwrapping of the redundant single-look (residual topographic error-free) interferograms. Generation of the deformation time series.
8. Estimation of the deformation velocity from the time series.
9. Geocoding of the results.

Fig 1. Amplitude image indicating the location of the area of interest.

3. Results and discussion

The monitoring case study considered in this work concerns an urban area undergoing construction works involving underground water pumping, which can potentially induce subsidence in an area of approximately 1 km radius around the construction area, hereafter referred to as study area. A wider area of approximately 16 km^2, considered stable, was monitored.

In this work, the APS component of the phases is modelled using a linear model which, although very simple (more complex atmospheric filters could have been implemented), is quite an effective approach in the specific context of the work at hand. Besides, the deformation area is masked prior to estimating the APS. The assumption made in this study is that in a small area, such as the study area under analysis, the APS behaves like a plane. Figure 2 displays the autocorrelation function of an image phase characterized by a strong atmospheric signal (a) and the autocorrelation function of the same image phase after removing the linear atmospheric component (b). The standard deviation of the phase drops from 0.44 rad to 0.32 rad. The autocorrelation function crosses the axis at 90 pixels (i.e. at a distance of approximately 3600 m) before APS correction, while it crosses the axis at pixel 38 (i.e. at a distance of approximately 1500 m) after corrections.

The final processing was carried out with 43 images because, after APS correction, one of the images showed a rather strong phase variation in comparison with the other images. Therefore, this image, probably affected by strong local atmospheric artefacts, was discarded.

Table 1. Sentinel-1 dataset processed for this work.

#	Orbit	Date	#	Orbit	Date	#	Orbit	Date	#	Orbit	Date
1	6132	20150529	**12**	8757	20151125	**23**	10682	20160405	**34**	12782	20160827
2	6307	20150610	**13**	8932	20151207	**24**	10857	20160417	**35**	12957	20160908
3	6657	20150704	**14**	9107	20151219	**25**	11032	20160429	**36**	13132	20160920
4	6832	20150716	**15**	9282	20151231	**26**	11207	20160511	**37**	13482	20161014
5	7007	20150728	**16**	9457	20160112	**27**	11382	20160523	**38**	13657	20161026
6	7357	20150821	**17**	9632	20160124	**28**	11557	20160604	**39**	13832	20161107
7	7707	20150914	**18**	9807	20160205	**29**	11907	20160628	**40**	14007	20161119
8	7882	20150926	**19**	9982	20160217	**30**	12082	20160710	**41**	14182	20161201
9	8057	20151008	**20**	10157	20160229	**31**	12257	20160722	**42**	14357	20161213
10	8407	20151101	**21**	10332	20160312	**32**	12432	20160803	**43**	14532	20161225
11	8582	20151113	**22**	10507	20160324	**33**	12607	20160815			

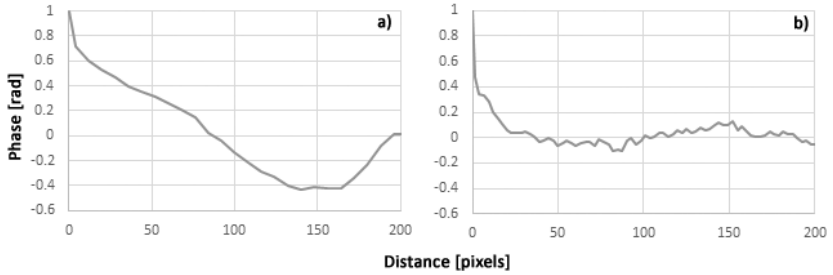

Fig. 2. (a) Autocorrelation function of a phase with APS; (b) Autocorrelation function after APS correction.

The linear deformation velocity and RTE were estimated after the APS correction. The RTE was subsequently removed from the interferograms and the time series were then calculated using the 2+1D phase unwrapping. The deformation velocity was finally estimated from the time series. Figure 3 shows an example of deformation velocity map, in which the spatial density of the Sentinel-1 based measurements can be appreciated. In general, the area shown in Figure 3 is stable. Moreover, the time series of two Persistent Scatterers (PSs) are shown.

The PS located at the lower left part of Fig. 3 displays deformation moving away from the satellite, which accumulates approximately 6 mm in the radar line-of-sight. Notwithstanding the rather noisy appearance of the time series, the deformation pattern is well-defined. In addition, the point is also clearly visible in the deformation velocity map.

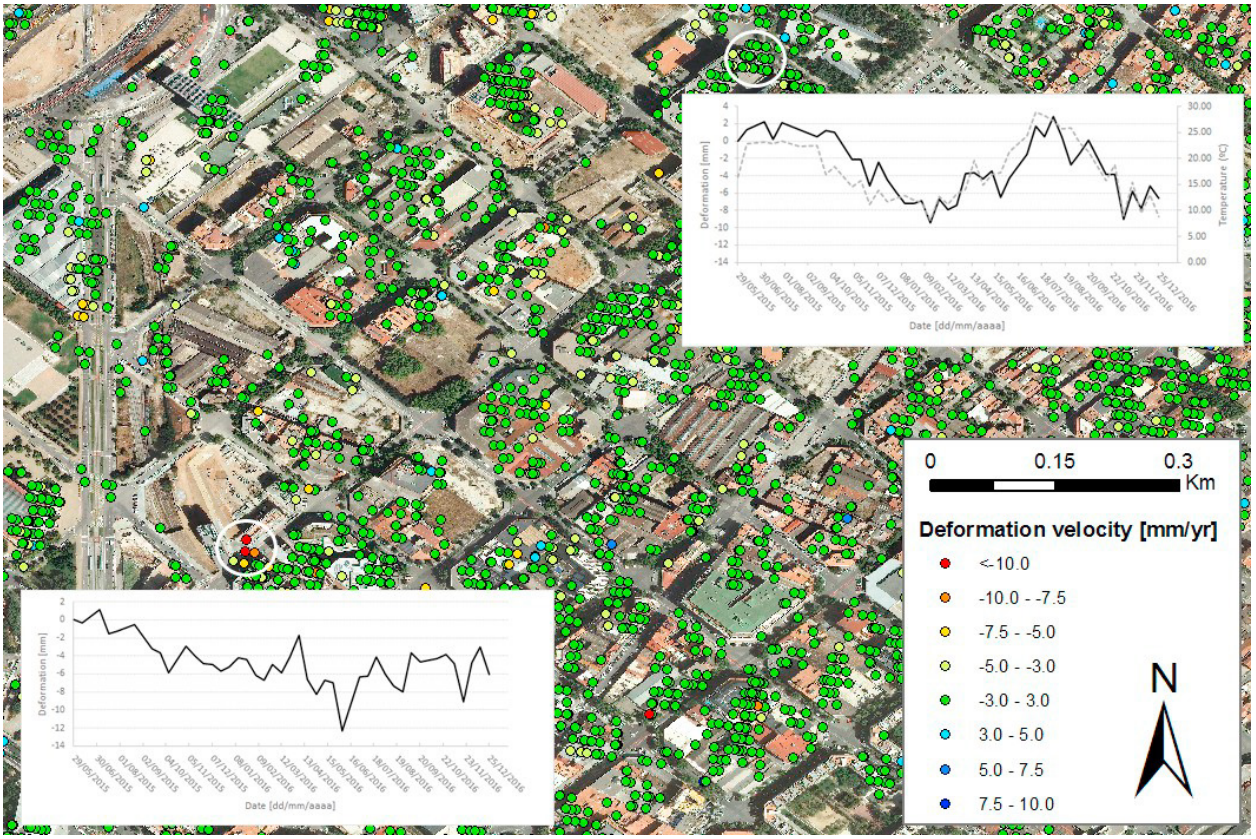

Fig. 3. Deformation velocity map displaying a portion of the area of interest. The time series of two Persistent Scatterers are shown.

The PS located at the upper right part of Fig. 3 shows a more complex deformation pattern, which is approximately sinusoidal. It is worth noting that this PS correctly seems as "stable" in the deformation velocity map. This point shows displacements caused by thermal expansion. This is evident by considering the plot of the temperature of the area of interest in correspondence to the time of acquisition of the Sentinel-1 images (Fig. 3. Upper right graph). The black (displacement) and grey (temperature) lines show a strong temporal correlation. This example illustrates the deformation monitoring potential of medium resolution Sentinel-1 data.

Acknowledgements

This work has been partially funded by the Spanish Ministry of Economy and Competitiveness through the DEMOS project "Deformation monitoring using Sentinel-1 data" (Ref: CGL2017-83704-P).

References

[1] Barra, A., Monserrat, O., Mazzanti, P., Esposito, C., Crosetto, M., Scarascia Mugnozza, G. (2016) "First insights on the potential of Sentinel-1 for landslides detection." *Geomatics, Natural Hazards and Risk* **7** (**6**): 1874–1883.

[2] Barra, A., Monserrat, O., Crosetto, M., Cuevas-Gonzalez, M., Devanthéry, N., Luzi, G., Crippa, B. (2017) "Sentinel-1 data analysis for landslide detection and mapping: first experiences in Italy and Spain." Proc. of Workshop on World Landslide Forum, 201-208. Springer, Cham.

[3] Biescas E., Crosetto M., Agudo M., Monserrat O., Crippa B. (2007) "Two radar interferometric approaches to monitor slow and fast land deformations." *Journal of Surveying Engineering* **133** (**2**): 66–71.

[4] Crosetto M., Tschthe erning C.C., Crippa B., Castillo M. (2002) "Subsidence Monitoring using SAR interferometry: reduction of the atmospheric effects using stochastic filtering." *Geophysical Research Letters* **29** (**9**): 26–29.

[5] Crosetto, M., Monserrat, O., Iglesias, R., Crippa, B. (2010) "Persistent Scatterer Interferometry: potential, limits and initial C- and X-band comparison." *Photogrammetric Engineering & Remote Sensing* **76** (**9**): 1061–1069.

[6] Crosetto, M., Monserrat, O., Luzi, G., Cuevas-González, M., Devanthéry, N. (2014) "Discontinuous GBSAR deformation monitoring." *ISPRS Journal of Photogrammetry and Remote Sensing* **93**: 136–141.

[7] Crosetto, M., Devanthéry, N., Cuevas-González, M., Monserrat, O., Crippa, B. (2015) "Exploitation of the full potential of PSI data for subsidence monitoring." Proc. of Nisols, Ninth International Symposium on Land Subsidence, 15-19 November 2015, Nagoya (Japan). Proc. IAHS, **372**: 311–314, doi:10.5194/piahs-372-311-2015, 2015.

[8] Crosetto, M., Monserrat, O., Cuevas-González, M. Devanthéry, N., Crippa, B. (2016) "Persistent Scatterer Interferometry: a review." *ISPRS Journal of Photogrammetry and Remote Sensing* **115**: 78–89.

[9] Dai, K., Li, Z., Tomás, R., Liu, G., Yu, B., Wang, X., Cheng. H. Chen, J., Stockamp, J. (2016) "Monitoring activity at the Daguangbao mega-landslide (China) using Sentinel-1 TOPS time series interferometry." *Remote Sensing of Environment* **186**: 501–513.

[10] De Luca, C., Bonano, M., Casu, F., Fusco, A., Lanari, R., Manunta, M., Zinno, I. (2016) "Automatic and Systematic Sentinel-1 SBAS-DInSAR Processing Chain for Deformation Time-series Generation." *Procedia Computer Science* **100**: 1176–1180.

[11] Devanthéry, N., Crosetto, M., Monserrat, O., Cuevas-González, M., Crippa, B. (2014) "An approach to Persistent Scatterer Interferometry." *Remote Sensing* **6**: 6662–6679.

[12] Ferretti, A., Prati, C., Rocca, F. (2001) "Permanent scatterers in SAR interferometry." *IEEE Transactions on Geoscience and Remote Sensing*, **39** (**1**): 8–20.

[13] Gernhardt, S., Bamler, R. (2012) "Deformation monitoring of single buildings using meter-resolution SAR data in PSI." *ISPRS Journal of Photogrammetry and Remote Sensing* **73**: 68–79.

[14] González, P. J., Bagnardi, M., Hooper, A.J., Larsen, Y., Marinkovic, P., Samsonov, S.V., Wright, T.J. (2015) "The 2014–2015 eruption of Fogo volcano: Geodetic modeling of Sentinel-1 TOPS interferometry." *Geophysical Research Letters* **42** (**21**): 9239–9246.

[15] Huang, Q., Crosetto, M., Monserrat, O., & Crippa, B. (2017) "Displacement monitoring and modelling of a high-speed railway bridge using C-band Sentinel-1 data." *ISPRS Journal of Photogrammetry and Remote Sensing* **128**: 204–211.

[16] Lan, H., Li, L., Liu, H., Yang, Z. (2012) "Complex urban infrastructure deformation monitoring using high resolution PSI." *J. Selected Topics in Applied Earth Observations and Remote Sensing* **5** (**2**): 643–651.

[17] Shirzaei, M., Bürgmann, R., Fielding, E. J. (2017) "Applicability of Sentinel-1 Terrain Observation by Progressive Scans multitemporal interferometry for monitoring slow ground motions in the San Francisco Bay Area." *Geophysical Research Letters* **44** (**6**): 2733–2742.

[18] Strozzi, T., Teatini, P., Tosi, L. (2009) "TerraSAR-X reveals the impact of the mobile barrier works on Venice coastland stability." *Remote Sensing of Environment* **113** (**12**): 2682–2688.